1-1-2009

Multifractal analysis of geomagnetic storm and solar flare indices and their class dependence

Zu-Guo Yu

Vo Anh
University of Central Florida

Richard Eastes
University of Central Florida

Multifractal analysis of geomagnetic storm and solar flare indices and their class dependence

Zu-Guo Yu,[1,2] Vo Anh,[1,3] and Richard Eastes[3]

Received 30 October 2008; revised 23 February 2009; accepted 19 March 2009; published 23 May 2009.

[1] The multifractal properties of two indices of geomagnetic activity, D_{st} (representative of low latitudes) and a_p (representative of the global geomagnetic activity), with the solar X-ray brightness, X_l, during the period from 1 March 1995 to 17 June 2003 are examined using multifractal detrended fluctuation analysis (MF-DFA). The $h(q)$ curves of D_{st} and a_p in the MF-DFA are similar to each other, but they are different from that of X_l, indicating that the scaling properties of X_l are different from those of D_{st} and a_p. Hence, one should not predict the magnitude of magnetic storms directly from solar X-ray observations. However, a strong relationship exists between the classes of the solar X-ray irradiance (the classes being chosen to separate solar flares of class X-M, class C, and class B or less, including no flares) in hourly measurements and the geomagnetic disturbances (large to moderate, small, or quiet) seen in D_{st} and a_p during the active period. Each time series was converted into a symbolic sequence using three classes. The frequency, yielding the measure representations, of the substrings in the symbolic sequences then characterizes the pattern of space weather events. Using the MF-DFA method and traditional multifractal analysis, we calculate the $h(q)$, $D(q)$, and $\tau(q)$ curves of the measure representations. The $\tau(q)$ curves indicate that the measure representations of these three indices are multifractal. On the basis of this three-class clustering, we find that the $h(q)$, $D(q)$, and $\tau(q)$ curves of the measure representations of these three indices are similar to each other for positive values of q. Hence, a positive flare storm class dependence is reflected in the scaling exponents $h(q)$ in the MF-DFA and the multifractal exponents $D(q)$ and $\tau(q)$. This finding indicates that the use of the solar flare classes could improve the prediction of the D_{st} classes.

Citation: Yu, Z.-G., V. Anh, and R. Eastes (2009), Multifractal analysis of geomagnetic storm and solar flare indices and their class dependence, *J. Geophys. Res.*, *114*, A05214, doi:10.1029/2008JA013854.

1. Introduction

[2] An important aim of solar-terrestrial physics is understanding the causes of geomagnetic activity in general and geomagnetic storms in particular. Although coronal mass ejections (CME) are the clear cause of most major geomagnetic storms [*Schwenn et al.*, 2005; *Yermolaev et al.*, 2005; *Zhang et al.*, 2007], they are difficult to observe or predict. Since solar flares are coincident with many CMEs [see, e.g., *Zhang et al.*, 2007], they are useful for prediction of geomagnetic storms [*Park et al.*, 2002; *Yermolaev et al.*, 2005] owing to the shorter propagation times of solar photons. In a recent study, *Howard and Tappin* [2005] found a dependence relationship between the classes of solar flare (using X-ray measurements from GOES) and geomagnetic storm (using the D_{st} and a_p indices) based on the statistics from 103 events. However, in another analysis, Y. I. Yermolaev and M. Y. Yermolaev (Geomagnetic storm dependence on the solar flare class, arXiv:physics/0601197.20062006, 2006), suggested that only a slight positive correlation between the classes of solar flare and geomagnetic storm is likely to be observed under more typical conditions. Yermolaev and Yermolaev (online article, 2006, pp. 1) argued that the conclusion by *Howard and Tappin* [2005, pp. 380] that "there is a tendency for large flares to be associated with very large storms" would be too strong, and maintained that "the class of solar flares could not predict the magnitude of magnetic storm". In this paper, we look into the flare storm dependence issue more rigorously using the tools of multifractal analysis. In fact, we convert the time series of X_l, D_{st}, and a_p into symbolic sequences (as described in section 2) in which an event is a string or a word in the symbolic sequence. We then study the dependence relationship of the indices in the form of symbolic sequences via (1) their representations as probabilities of occurrence of events (K strings) and (2) the multiscaling properties of these representations. This approach provides more detailed information on the relation-

[1]School of Mathematical Sciences, Queensland University of Technology, Brisbane, Queensland, Australia.
[2]School of Mathematics and Computational Science, Xiangtan University, Hunan, China.
[3]Florida Space Institute, University of Central Florida, Orlando, Florida, USA.

0148-0227/09/2008JA013854

ship between solar flares, as seen in the solar X rays and geomagnetic disturbances than traditional correlation studies. Our results support the finding of *Howard and Tappin* [2005].

[3] While the studies mentioned above have focused on a relatively small number of events, ~10 per year with large magnitudes, the analyses performed in this paper utilize hourly data over the period March 1995 to June 2003. Consequently, contributions from corotating interaction regions (CIRs) are included. The use of hourly data also helps avoid biasing the results through the data selection process. The period used overlaps with the period from which *Howard and Tappin* [2005] selected, namely January 1998 to August 2004, but their analysis concentrated on 103 events. The more recent study described by *Zhang et al.* [2007] also used data from a similar period, January 1996 to December 2005, and concentrated on 88 events. From existing flare and solar wind observations, a unique association of CME to interplanetary coronal mass ejection (ICME) can be observed for only about half of all ICME events [*Zhang et al.*, 2007], primarily because of the difficulty in making one-to-one correspondence with events on the Sun, owing to the complexity of interplanetary flows. With the techniques used in the following analysis, significant insights can be obtained even without establishing the one-to-one correspondence.

[4] In the following analysis, fractal methods are used to characterize the scaling properties in each time series. Multifractal analysis was initially proposed to treat turbulence data and is a useful way to characterize the spatial heterogeneity of both theoretical and experimental fractal patterns [*Grassberger and Procaccia*, 1983; *Halsy et al.*, 1986]. Fractal and multifractal approaches have been quite successful in extracting salient features of physical processes responsible for the near-Earth magnetospheric phenomena in the recent literature [*Lui*, 2002]. Examples include a method to describe the multiple scaling of the measure representation of the D_{st} time series provided by *Wanliss et al.* [2005]; a prediction method based on the recurrent iterated function system in fractal theory detailed by *Anh et al.* [2005] together with some evaluation of its performance; and a two-dimensional chaos game representation of the D_{st} index for prediction of geomagnetic storm events was proposed by *Yu et al.* [2007].

[5] *Peng et al.* [1994] introduced the detrended fluctuation analysis (DFA), which has become a widely used technique to determine the fractal scaling properties of, and to detect the long-range correlations in, stationary and nonstationary time series [*Hu et al.*, 2001; *Chen et al.*, 2002]. The multifractal detrended fluctuation analysis (MF-DFA) proposed by *Kantelhardt et al.* [2002] is a modified version of the DFA to detect multifractal properties of time series. It allows a reliable multifractal characterization of nonstationary time series typical of geophysical phenomena [*Kantelhardt et al.*, 2002].

[6] In this paper, we use MF-DFA and traditional multifractal analysis to study the scaling properties of D_{st}, a_p, and the solar X-ray measurements from the Geostationary Operational Environmental Satellites (GOES) during the March 1995 to June 2003 period. These analyses indicate that there are significant similarities between the scaling properties of the classes of geomagnetic disturbances and those of X-ray flare brightness which have not been previously identified. It should be possible to use these similarities to improve the prediction of classes of storms using classes of solar X-ray measurements.

2. Data

[7] The solar X-ray data used are hourly measurements from the GOES space environment monitor. Data from GOES 6, 7, 8, 9, 10, 11, and 12 were downloaded from the National Geophysical Data Center (NGDC, http://spidr.ngdc.noaa.gov/spidr/index.jsp) and combined, using the later satellites to fill, whenever possible, any gaps in the data from the earlier satellites. No attempt was made to compensate for differences in calibration between the measurements or to average the measurements. By using multiple satellites, gaps in the observations are reduced significantly. During the period covered by GOES 8 (1 March 1995 to 30 June 2003) the number of hours where observations are unavailable is reduced from 1496 to 77 for the longer wavelength, X_l, observations (1–8 Å). Most of the remaining gaps in the hourly measurements span multiple hours, even a full 24 h. Since they are present even though there are usually three satellites providing observations, they are probably the result of geomagnetic storm effects at Earth. Although the solar measurements may be missing during a storm, any flare(s) associated with a storm is typically observed, since it occurred hours earlier.

[8] The hourly D_{st} time series and the interpolated hourly (originally 3 hourly) time series of a_p for the period 1 March 1995 to June 2003 were downloaded from the SPIDR Web site. Both of the geomagnetic indices and the X_l data are shown in Figure 1.

[9] The empirical probability densities of the three indices are plotted in Figure 2 (left). From the top and bottom plots in Figure 2 (left), we see that the empirical probability densities of a_p and X_l have the shape of the inverse Gaussian distribution whose density is of the form [*Chhikara and Folks*, 1989]

$$f(x;\lambda,\mu) = \left(\frac{\lambda}{2\pi}\right)^{1/2} x^{-3/2} \exp\left\{-\frac{1}{2}\frac{\lambda(x-\mu)^2}{\mu^2 x}\right\} \mathbf{1}_{(0,\infty)}(x),\ \mu > 0, \lambda > 0.$$

[10] A method to estimate the parameters μ and λ in the inverse Gaussian distribution is given by *Chhikara and Folks* [1989], and *Anh et al.* [2008]. Here the estimated values of μ and λ are 12.3849 and 11.4611 for a_p, 9.9716e-007 and 2.9793e-008 for X_l respectively. But the inverse Gaussian distribution does not fit well the empirical probability density of D_{st}. Hence, we propose to use the α-stable distribution. A Lévy skew α-stable distribution or just stable distribution is specified by the scale parameter γ, exponent α, shift δ and skewness parameter β. The exponent α controls the kurtosis and must lie in the range (0,2]. The value $\alpha = 2$ corresponds to a Gaussian distribution (for any β), while the values $\alpha = 1$, $\beta = 0$ correspond to a Cauchy distribution. The skewness parameter β must lie in the range $[-1, 1]$ and when it is zero, the distribution is symmetric and is referred to as a Lévy symmetric α-stable distribution. The scale parameter γ must be larger than zero and equals to

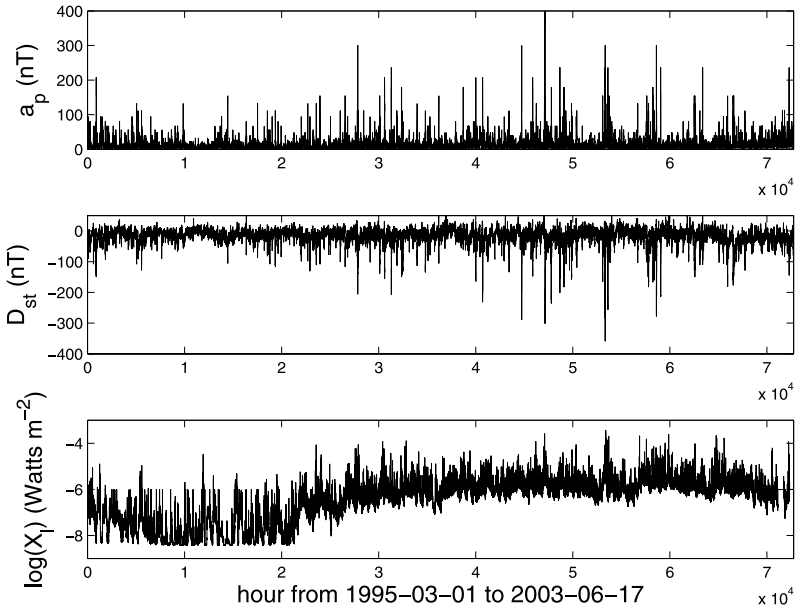

Figure 1. The hourly time series of the D_{st}, a_p, and X_l indices from 1 March 1995 to 17 June 2003.

half the variance in that Gaussian case (i.e., when $\alpha = 2$). The shift δ is a location parameter, which is the mean when $1 < \alpha \leq 2$ and the median when $0 < \alpha < 1$ [*NiKias and Shao*, 1995]. The Lévy skew stable probability distribution is defined by the Fourier transform of its characteristic function [*Nolan*, 2009]:

$$f(x;\alpha,\beta,\gamma,\delta) = \int_{-\infty}^{\infty} \varphi(x) e^{-itx} dt,$$

where $\varphi(t)$ is given by

$$\varphi(t) = \exp\{i\delta t - \gamma|t|^{\alpha}[1 + i\beta sign(t) w(t,\alpha)]\},$$

and

$$w(t,\alpha) = \begin{cases} \tan\frac{\alpha\pi}{2}, & \text{if} \quad \alpha \neq 1, \\ \frac{2}{\pi}\log|t|, & \text{if} \quad \alpha = 1, \end{cases}$$

$$sign(t) = \begin{cases} 1, & \text{if} \quad t > 0, \\ 0, & \text{if} \quad t = 0, \\ -1, & \text{if} \quad t < 0. \end{cases}$$

We use the maximum likelihood method to estimate the parameters α, β, γ and δ in the α-stable distribution and fit the empirical probability density function (PDF) of the D_{st} time series. The estimated parameters are $\alpha = 1.5944$, $\beta = -0.9053$, $\gamma = 10.8678$ and $\delta = -10.0418$. From the middle plot in Figure 2 (left), it is seen the α-stable density fits well the empirical PDF of the D_{st}. But similar exercises indicate that the α-stable density does not fit the empirical densities of a_p and X_l. These fittings confirm that a_p, D_{st} and X_l are all non-Gaussian. The heavy tail behavior is more pronounced in the log form of these densities (see Figure 2 (right)). The presence of this non-Gaussianity in the time series of a_p, D_{st} and X_l suggests that the traditional multifractal analysis is not appropriated for a study of their scaling. Instead, a multifractal detrended fluctuation analysis (described in section 4.2) will be suggested and performed on these time series.

3. Measure Representation Based on Classes

[11] In this paper, we also examine the multiple scaling of the time series via their measure representation. We outline here the method [*Yu et al.*, 2001a] used in deriving the measure representation of each time series. First we define a map f_1 as follows.

[12] For the D_{st} time series, in nanoTeslas (nT),

$$f_1 = \begin{cases} 0, & \text{if} \quad D_{st} \geq -30, \\ 1, & \text{if} \quad -50 < D_{st} < -30, \\ 2, & \text{if} \quad D_{st} \leq -50. \end{cases}$$

Because there are only a few big storms in the time period analyzed, they are grouped with the medium storms into one class. Therefore, the values 2, 1 and 0 correspond to medium or large storms, small storms, and quiet conditions respectively in map f_1, which was described and used by *Anh et al.* [2005].

[13] For the a_p time series, in nT,

$$f_1 = \begin{cases} 0, & \text{if} \quad a_p \leq 30, \\ 1, & \text{if} \quad 30 < a_p < 60, \\ 2, & \text{if} \quad a_p \geq 60, \end{cases}$$

according to the classification of a_p given in Table 1 of *Howard and Tappin* [2005].

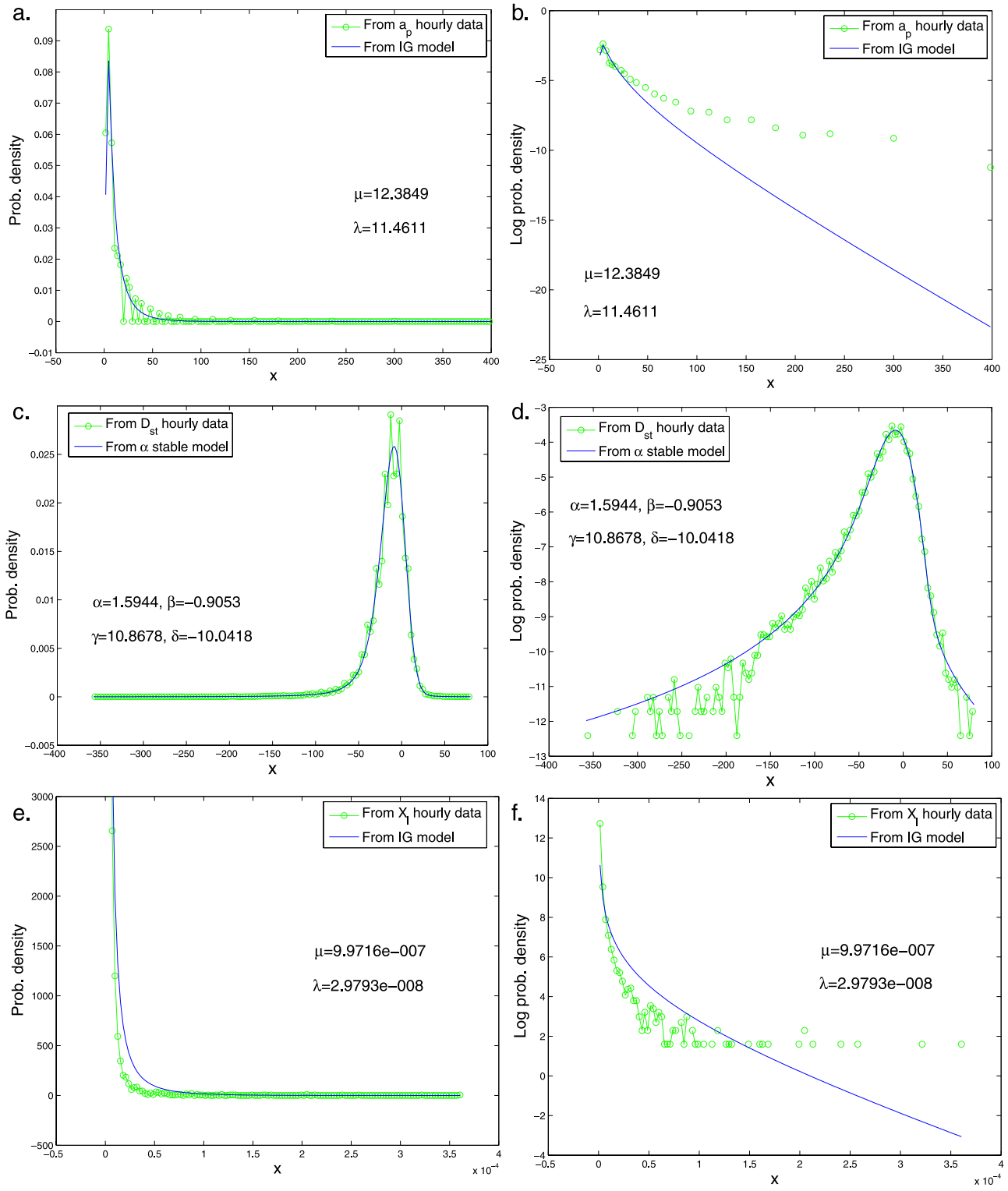

Figure 2. (left) Empirical probability densities and the fitted curves from an inverse Gaussian density or α -stable density for D_{st}, a_p, and X_l. (right) The log form of the probability densities on the left.

[14] For the X_l time series, in Wm^{-2},

$$f_1 = \begin{cases} 0, & \text{if} \quad X_l \le 10^{-6}, \\ 1, & \text{if} \quad 10^{-6} < X_l < 10^{-5}, \\ 2, & \text{if} \quad X_l \ge 10^{-5}, \end{cases}$$

according to the classification of X_l given on the web page http://www.spaceweather.com/glossary/flareclasses.html. The values 2, 1, and 0 correspond to flares of class M or X; class C; and class B of smaller flares (including times when there are no flares) respectively in map f_1.

[15] Using map f_1, we convert the D_{st}, a_p, and X_l time series into symbolic sequences with alphabet {0, 1, 2}. We call any string made up of K numbers from the set {0, 1, 2} a K string. For a given K there are in total 3^K different K strings, and 3^K counters are needed to count the number of K strings in a given time series. We divide the interval [0,1) into 3^K disjoint subintervals, and use each subinterval to represent a counter. Letting $\eta = \eta_1 \ldots \eta_K$, $\eta_i \in \{0, 1, 2\}$, $i = 1,\ldots,K$, be a substring with length K, we define

$$x_l(\eta) = \sum_{i=1}^{K} \frac{\eta_i}{3^i}, \qquad x_r(\eta) = x_l(\eta) + \frac{1}{3^k}.$$

[16] We then use the subinterval $[x_l(\eta), x_r(\eta))$ to represent the substring η. Let $N(\eta)$ be the number of times a substring η appears in the time series counted by a sliding window with width K (sliding one position each time along the symbolic sequence). If the time series has length L, we define $F(\eta) = N(\eta)/(L-K+1)$ to be the frequency of substring η. It follows that $\Sigma_{\{\eta\}} F(\eta) = 1$. We can now view $F(\eta)$ as a function of x and define a measure ν on [0,1) by $\nu(x) = g(x)\,dx$, where $g(x) = 3^K F(\eta)$, $x \in [x_l(\eta), x_r(\eta))$. We call ν the measure representation of the given time series. It is noted that this histogram-type representation will have a different shape according to the order of the K strings on the interval [0,1), but it is unique for each time series once this order is fixed (usually the dictionary order is used). This concept is an extension of the usual histogram, where each substring consists of a single value.

[17] As examples, the measure representations of the active and quiet periods of a_p, D_{st} and X_l with $K = 8$ using map f_1 are plotted in Figure 3. The presence of the same substrings in the a_p and D_{st} series as seen in the active period of the X_l time series may indicate a dependence on the X_l time series.

4. Multifractal Analyses

4.1. Traditional Multifractal Analysis

[18] The most common algorithms of traditional multifractal analysis are the so-called fixed size box-counting algorithms [*Halsy et al.*, 1986]. In the one-dimensional case, for a given measure ν with support $E \subset R$, we consider the partition sum

$$Z_\epsilon(q) = \sum_{\nu(B)\neq 0} [\nu(B)]^q, \tag{1}$$

$q \in R$, where the sum is evaluated over all different nonempty boxes B of a given side ϵ in a grid covering of the support E:

$$B = [k\epsilon, (k+1)\epsilon). \tag{2}$$

The exponent $\tau(q)$ is defined by

$$\tau(q) = \lim_{\epsilon\to 0} \frac{\ln Z_\epsilon(q)}{\ln \epsilon}, \tag{3}$$

and the generalized fractal dimensions of the measure are defined as

$$D(q) = \tau(q)/(q-1), \text{ for } q \neq 1, \tag{4}$$

and

$$D(q) = \lim_{\epsilon\to 0} \frac{Z_{1,\epsilon}}{\ln \epsilon}, \text{ \% for } q = 1, \tag{5}$$

where $Z_{1,\epsilon} = \Sigma_{\nu(B)\neq 0} \nu(B) \ln \nu(B)$. The generalized fractal dimensions are numerically estimated through a linear regression of $(\ln Z_\epsilon(q))/(q-1)$ against $\ln \epsilon$ for $q \neq 1$, and similarly through a linear regression of $Z_{1,\epsilon}$ against $\ln \epsilon$ for $q = 1$. The value $D(1)$ is called the information dimension and $D(2)$ the correlation dimension. The $D(q)$ corresponding to positive values of q give relevance to the regions where the measure value is large. The $D(q)$ corresponding to negative values of q deal with the structure and the properties of the regions where the measure value is small.

[19] If the $\tau(q)$ curve is a straight line, we infer that the time series is a monofractal process, otherwise it is a multifractal process.

4.2. Multifractal Detrended Fluctuation Analysis

[20] The traditional multifractal analysis has been developed for the multifractal characterization of normalized, stationary time series. This standard formalism does not give correct results for nonstationary time series which are affected by trends. Multifractal detrended fluctuation analysis, which is a generalization of the standard DFA, is based on the identification of the scaling of the qth-order moments of the time series, which may be nonstationary [*Kantelhardt et al.*, 2002]. DFA has been used to study the length sequences of complete genomes [*Yu et al.*, 2001b] and the classification problem of protein secondary structures [*Yu et. al.*, 2006]. *Movahed et al.* [2006] used the MF-DFA to study sunspot fluctuations. *Picoli et al.* [2007] used the DFA and MF-DFA to investigate the fractal and multifractal properties of D_{st}. *Anh et al.* [2007] also used the DFA and MF-DFA to study the orthogonal field components from the global INTERMAGNET stations.

[21] We first summarize the MF-DFA technique. Consider a time series $\{X_1, X_2, \ldots, X_N\}$ of length N. For an integer $s \geq 0$, we divide the time series into $[N/s]$ segments of equal length s, where $[N/s]$ is the integer part of N/s. In each segment j, we compute the partial sums $Y(i) = \Sigma_{k=1}^{i} X_k$, $i = 1,2,\ldots,s$, fit a local trend $y_j(i)$ to $Y(i)$ by least squares, then compute the sample variances of the residuals:

$$F^2(s,j) = \frac{1}{s}\sum_{i=1}^{s} \left(Y((j-1)s+i) - y_j(i)\right)^2, j = 1,\ldots,[N/s]. \tag{6}$$

Note that linear, quadratic, cubic, or higher-order polynomials $y_j(i)$ can be used in the local trend fitting, and the DFA is accordingly called DFA1, DFA2, DFA3,.. In the following we use only DFA1.

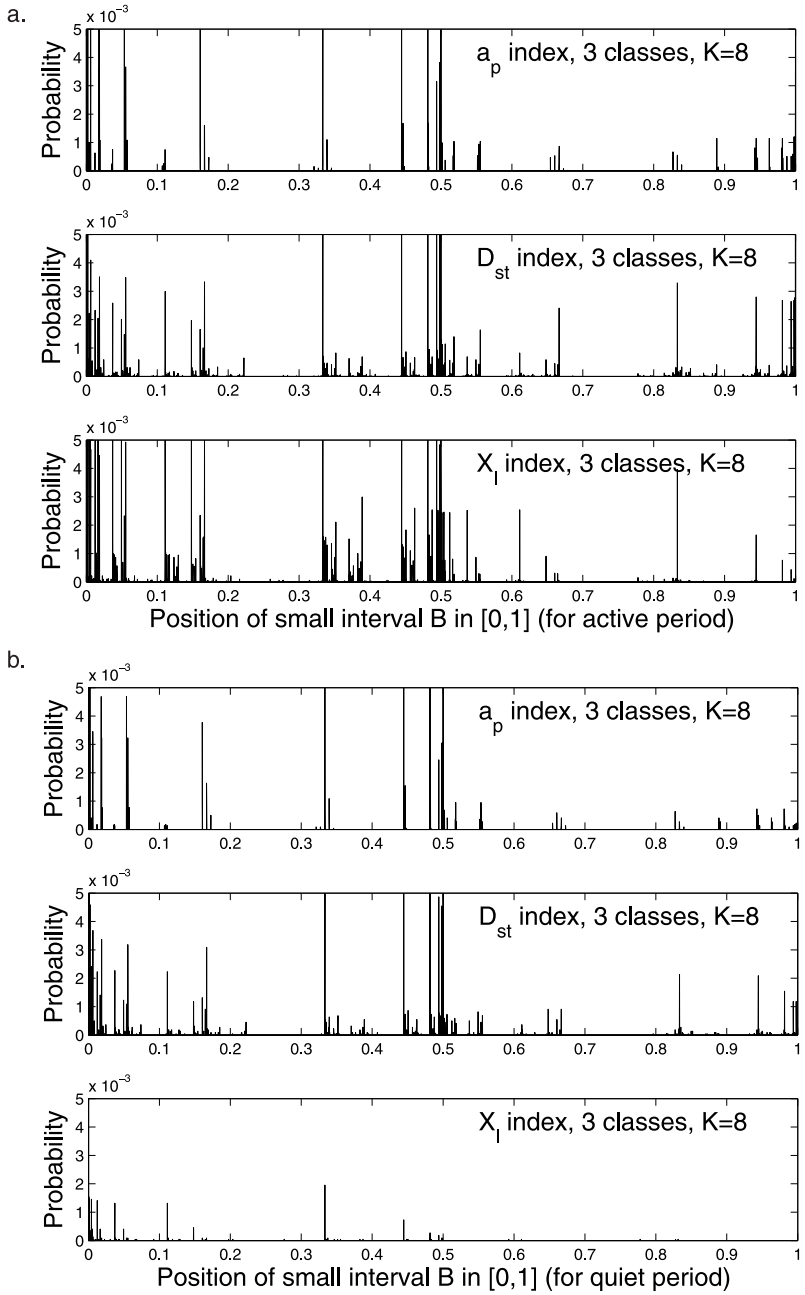

Figure 3. The measure representations of hourly D_{st}, a_p, and X_l with $K = 8$ using map f_1 from 1 March 1995 to 17 June 2003 for the (a) active and (b) quiet periods.

[22] The qth-order fluctuation function is then defined as the average over all segments:

$$F_q(s) = \left(\frac{1}{[N/s]} \sum_{j=1}^{[N/s]} \left(F^2(s,j) \right)^{q/2} \right)^{1/q}. \quad (7)$$

Since the segments are all of the same length, the second-order fluctuation function $F_2(s)$ is equivalent to the sample variance of the entire series. This is not so for the general case $q \neq 2$. We will assume that $F_q(s)$ is characterized by a power law:

$$F_q(s) \propto s^{h(q)}. \quad (8)$$

The scaling function $h(q)$ is then determined by the regression of log $F_q(s)$ on log s in some range of time scale s.

[23] For fractional Brownian motion, *Movahed et al.* [2006] showed that the Hurst index $H = h(2) - 1$. Using this relationship (or $H = h(2)$ for the stationarity case) and the estimate of $h(2)$ from the regression of log $F_2(s)$ on log

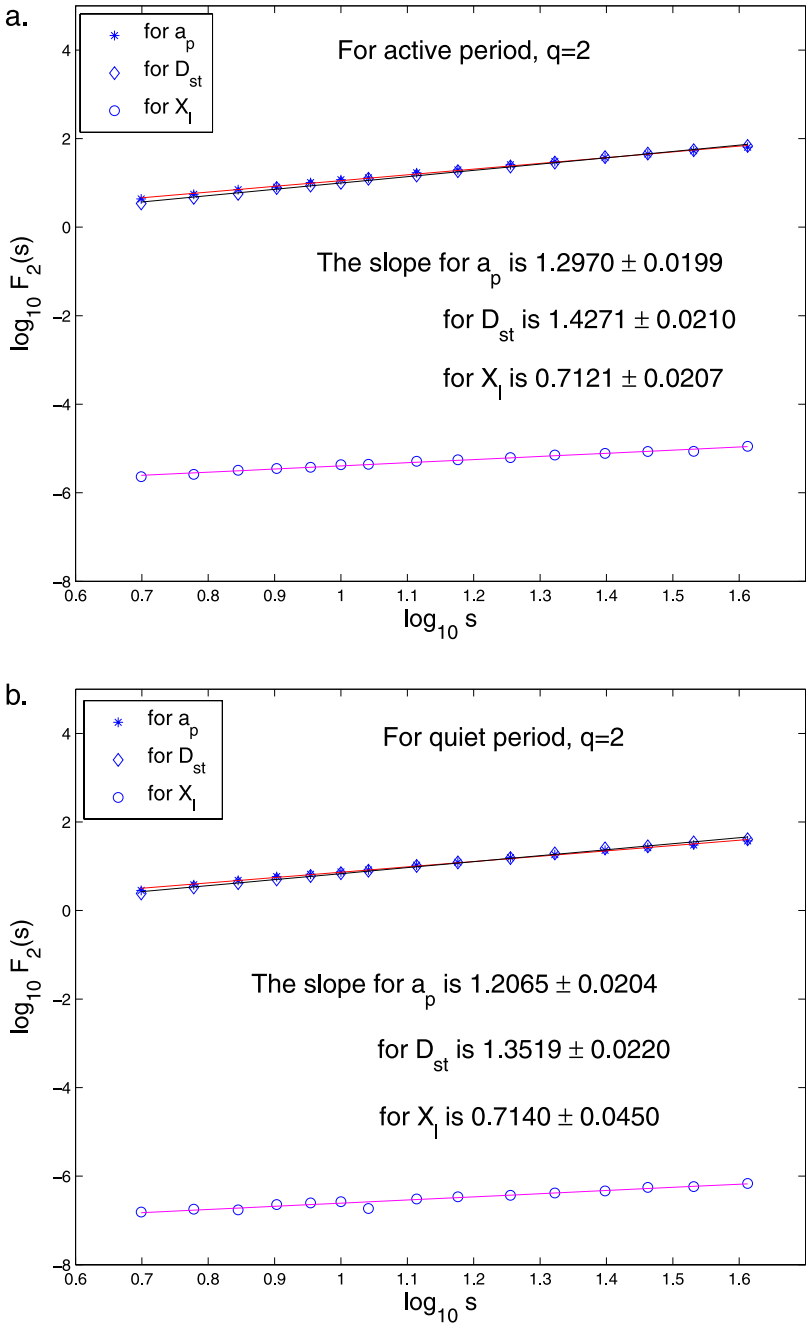

Figure 4. The log-log plots of $F_q(s)$ versus s of hourly a_p, D_{st}, and X_l from 1 March 1995 to 17 June 2003 for the (a) active and (b) quiet periods. The unit on the x axis is hour.

s, an estimate of the Hurst index H, and hence the extent of long memory in the time series, is obtained. For Brownian motion (with uncorrelated increments), the scaling exponent H is equal to 1/2. The range $1/2 < H < 1.0$ indicates the presence of long memory/persistence, while the range $0 < H < 1/2$ indicates short memory/antipersistence.

5. Data Analysis

[24] Using the multifractal analyses described in section 4, we will now examine the scaling properties of the D_{st} index, the X-ray flare brightness (X_l), and the a_p index during the period from 1 March 1995 to 17 June 2003. As seen in Figure 1, the behavior of X_l, at the earlier times, before $t = 22000$, differs from its behavior at the later times. The first will be referred to as the quiet period and the second as the active period. It is clear from an examination of the data that in the earlier, quiet period, the minimum values obtained were never below the sensitivity threshold of the instrument, which decreases the observed fluctuations in the data. Consequently, reliable conclusions about the behavior of the X-ray flares cannot be obtained from the earlier data. However, conclusions can be drawn from analysis of the later part of the time series.

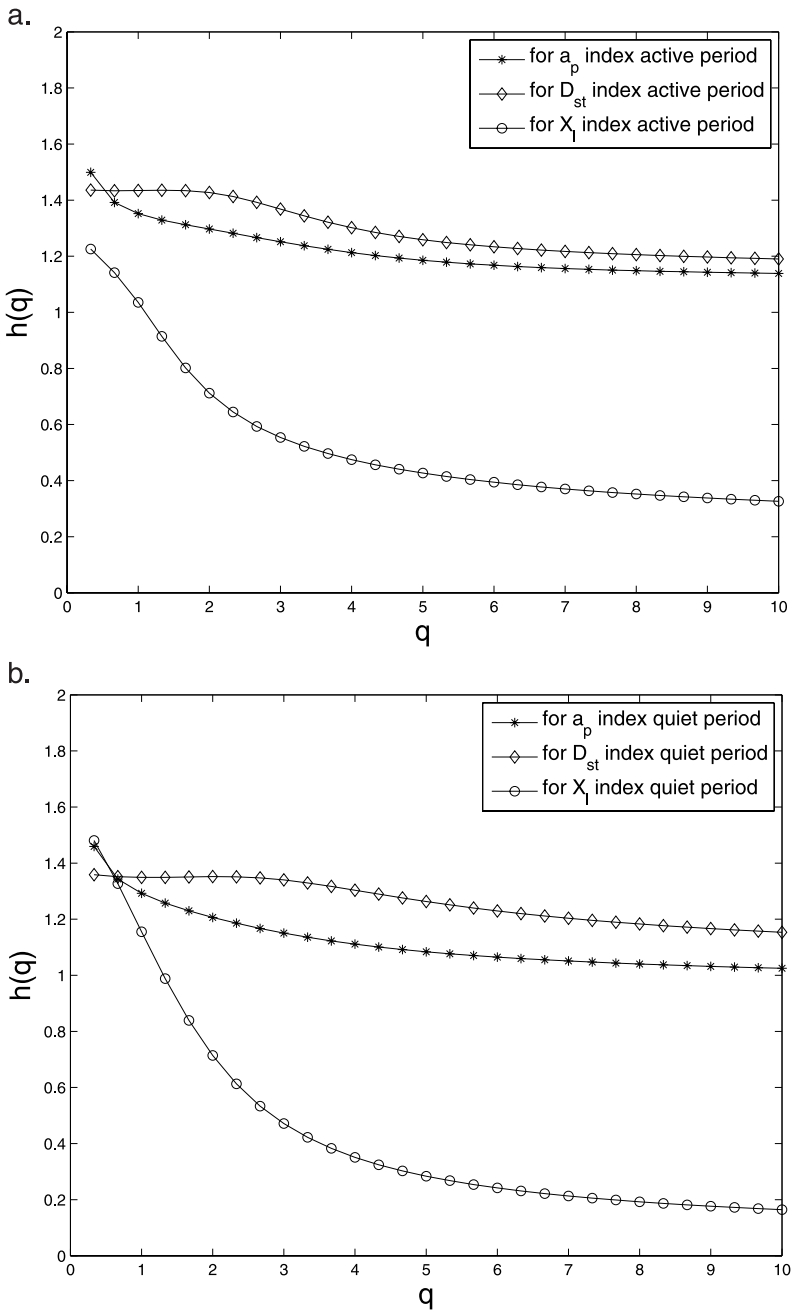

Figure 5. The $h(q)$ curves of hourly D_{st}, a_p, and X_l from 1 March 1995 to 17 June 2003 for the (a) active and (b) quiet periods.

[25] Because the traditional multifractal analysis cannot be used in a nonstationarity context indicated by Figure 4, which seems apparent for D_{st} and X, the MF-DFA technique is used to analyze the multifractal property of the three time series. Shown in Figure 5 are the results for the D_{st}, a_p and X_l time series during the active period using the MF-DFA1 method for small scales $5 < s < 34$. As seen in Figure 5, the curves for D_{st} and a_p have similar magnitudes and shapes throughout the range considered, indicating that their scaling properties are similar. Previous comparisons [e.g., *Jurac and Richardson*, 2001] of solar wind parameters indicated similar second-order correlations (0.6–0.9) for both D_{st} and a_p. The behavior of X_l differs significantly, indicating the scaling properties are different. Hence, the scaling behavior shown in Figure 5 indicates the prediction of magnetic storm magnitudes directly from flare observations would be imprecise, although a significant relationship may exist.

[26] In order to look at the scaling property for the flare storm class dependence problem, we used the measure representations of the three indices obtained from the map f_1 (for three classes). With regard to the value of K in the measure representations, if K is too small, there are not enough K strings to yield statistical meaning; on the other hand, if K is too large, many probabilities of occurrence of the K strings will be equal to 0, which is not suitable for analyses either. Here we take K from 6 to 10 for the three-

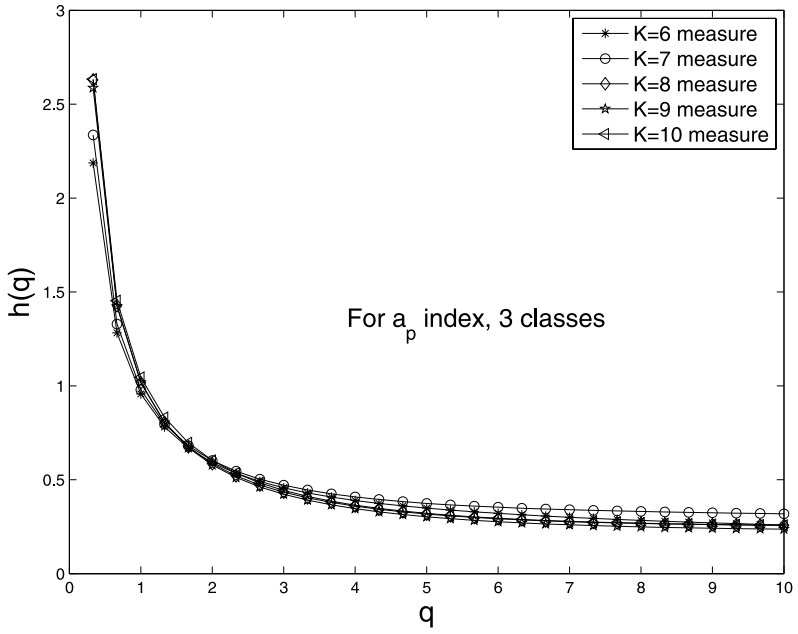

Figure 6. The $h(q)$ curves of the measure representations of the a_p index with different values of K in the three-class case.

class case. We can also regard these measure representations of D_{st}, a_p, and X_l as time series. Then the MF-DFA technique is used to detect their multifracal behavior as shown in Figure 6 for a_p for example. The $h(q)$ curves of the measure representations with different K values are close to each other. This means that the results will not be affected by the choice of K (for example, from 6 to 10 in the three-class case). Therefore, the $h(q)$ curves, for the three-class case with $K = 8$, are used for the measure representations of the three indices, which are shown in Figure 7.

[27] It is seen that the curves are close and similar to each other. In the measure representations, we consider only the classes of these three indices, not their magnitudes. This result indicates that the scaling exponents $h(q)$ in the MF-DFA reflect a positive dependence between the flare classes and the storm classes. Our results are consistent with the finding of *Howard and Tappin* [2005].

[28] In order to confirm that there is a positive flare storm class dependence, we also performed the traditional multifractal analysis on the measure representations of the three indices. We obtained $0.5 < h(2) < 1.0$ for the measure representations, indicating that they are stationary and normalized measures. Therefore, the traditional multifractal analysis is suitable. As examples, the $D(q)$ and $\tau(q)$ curves for the three-class case with $K = 8$ of the measure representations are shown in Figures 8 and 9.

[29] The curves $D(q)$ and τ (q) of the measure representations of the three indices are almost the same for positive q (i.e., for those frequent events or K strings). This confirms that there is a positive flare storm class dependence. For negative q (i.e., for those rare events or K strings), the $D(q)$ and τ (q) curves are the same for D_{st} and X_l in the active period but differ during the quiet period. This indicates that the changes in X_l are more closely related to those of D_{st} in the active period than in the quiet period. Since the instruments measuring X_l do not measure the lower X-ray irradiances during the quiet period, the relationship is weaker, as expected, during that period. There is also an indication that there is a statistically significant difference between the response of D_{st} and a_p to changes in X_l.

6. Discussion

[30] While the scaling behaviors of the time series of D_{st} and a_p (Figure 5) are similar and the behaviors for both differ from that of X_l, the scaling behavior of the measure representations gives different results. The scaling behaviors of the measure representations of D_{st} and X_l during the active period are similar, indicating these two have the closest relationship. The similarity of D_{st} and a_p shown in Figure 4, and the difference between their scaling behaviors and that of X_l is consistent with the solar wind being the primary influence for both. Although the solar wind varies with solar activity, solar flares are sufficiently localized that the solar wind is not expected to be dependent on their frequency. The similarity between the probability measures shown in Figure 3 for D_{st} and X_l during the active period indicates similar random patterns are present in both sets of data. The scaling behavior captured in the multifractal analysis is consistent with this conclusion. The results also indicate fractal techniques could be used for modeling this relationship.

[31] While the models currently used for prediction of D_{st} rely on solar wind observations and do not incorporate a dependence on solar flares, a dependence on flares is consistent with what is known about the effects of solar flares. Large flares affect both the neutral and ion densities, and the strongest changes, on the order of 50%, occur near the equator [e.g., *Mendillo et al.*, 1974; *Liu et al.*, 2007]. While most previous works concentrated on the largest flares, of magnitudes which occur only $\sim$10/year, short wavelength measurements indicate that small (class B)

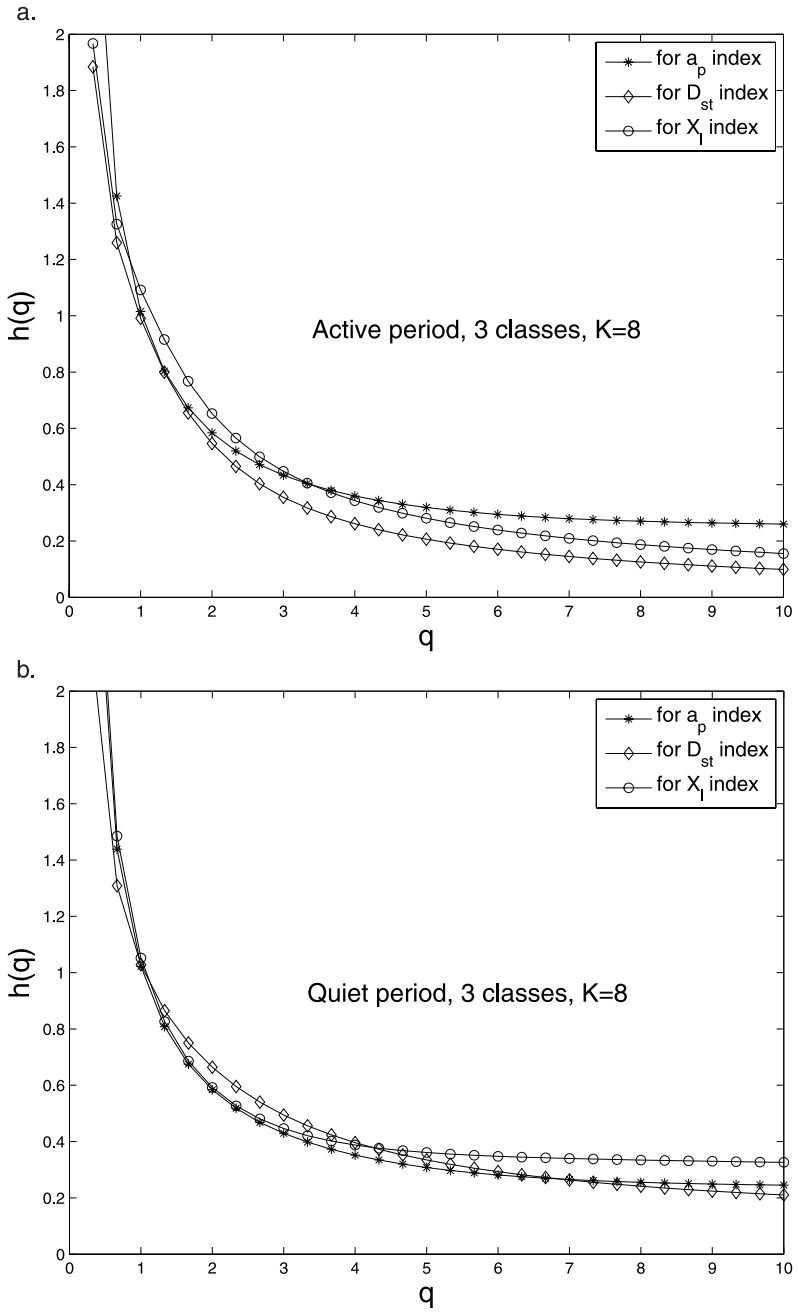

Figure 7. The $h(q)$ curves in the three-class case with $K = 8$ for the measure representations of D_{st}, a_p, and X_l for the (a) active and (b) quiet periods.

flares occur ~5 times each day (T. Woods, personal communication, 2007) and class C flares typically occur daily. Although the response of the thermosphere-ionosphere to small and medium flares is less than the response to the largest flares, medium sized flares are orders of magnitude more numerous and they would be expected to influence the neutral and ion densities, just as the large flares do. Although the use of hourly data decreases the sensitivity of the analysis to the smaller C class flares (the smallest used in the analysis), these flares play a dominant role in the results. Larger M and X class flares are lumped together since the frequency of the X class flares alone is too low for meaningful results. Regardless of the size of the flare, it heats the neutral atmosphere and increases the ion density. When the atmospheric expansion, which results from the heating, drives ions across the magnetic field, the electric fields within the thermosphere-ionosphere system are also affected. These changes should influence the D_{st} index. The analysis presented here indicates it does.

[32] The measure representations allow one to compare the behavior of different series, without the interdependence within the individual data series. By reducing each series to a limited number of discrete levels and looking for similar sequences of events one can identify whether the naturally occurring, random combinations of solar irradiance levels are also seen in D_{st} and a_p. While both D_{st} and a_p have a significant dependence on the solar wind, the results of the analysis show that the random pattern of solar irradiance

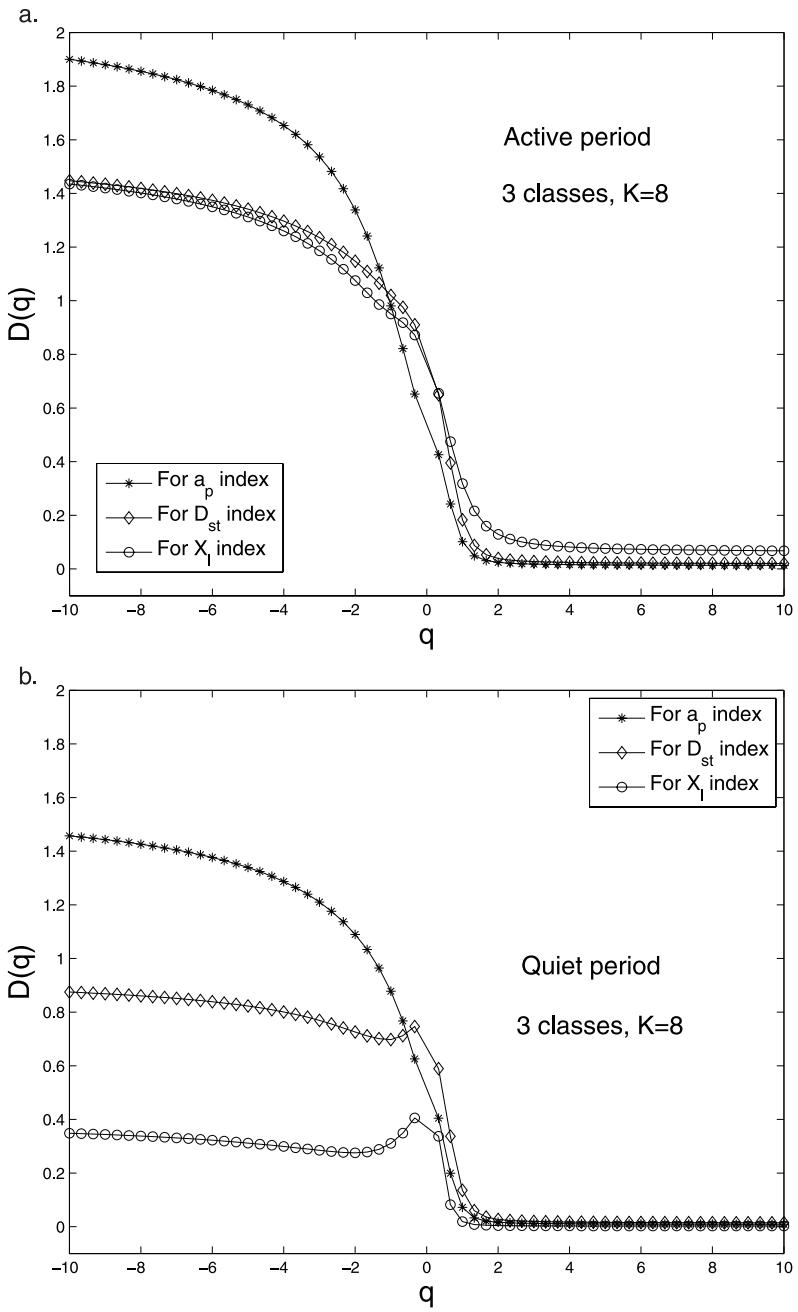

Figure 8. The $D(q)$ curves in the three-class case with $K = 8$ for the measure representations of D_{st}, a_p, and X_l for the (a) active and (b) quiet periods.

levels is seen more clearly in D_{st} than in a_p. This means D_{st} has a measurable dependence on the solar irradiance changes, in addition to its dependence on the solar wind. However, current models for D_{st} rely on solar wind parameters and have no dependence on the solar (X-ray) irradiance [e.g., *Temerin and Li*, 2002, 2006]. Owing to the sensitivity of D_{st} to changes in the solar irradiance, including it would improve the prediction of D_{st}.

7. Conclusions

[33] The analysis performed indicates there is a significant relationship between the classes of the solar X rays, X_l, and the D_{st} indices. This relationship is stronger than that seen between any other combination of the three indices X_l, D_{st}, and a_p. However, when comparing the raw data, D_{st} and a_p have the most significant relationship. The scaling properties (from the $h(q)$ curves) of D_{st} and a_p are similar and they differ substantially from that of X_l. Dramatically different results are obtained when using the measure representations. Using a three-level classification, for positive values of q (where the scaling behavior is more relevant for the high frequent events) the $h(q)$, $D(q)$, and $\tau(q)$ curves for all three indices are similar. And the scaling properties, as shown by the $D(q)$ and $\tau(q)$ curves for negative q (which represents the scaling behavior of the low frequent K strings or events), of the measure representations indicate the scaling behaviors of the D_{st} and X_l series

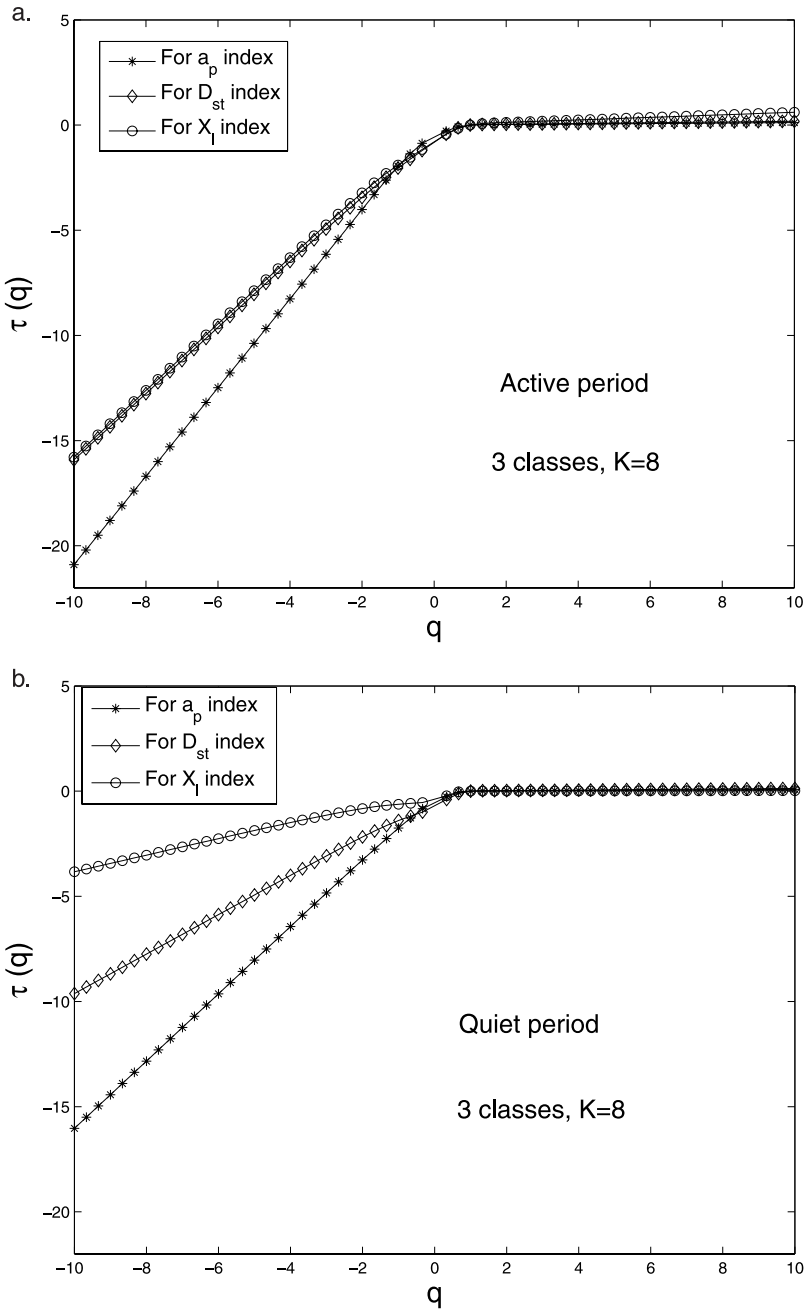

Figure 9. The τ (q) curves in the three-class case with $K = 8$ for the measure representations of D_{st}, a_p, and X_l for the (a) active and (b) quiet periods.

in the active period are similar. These suggests there is a significant relationship, for high frequent events in all three indices and for low frequent events in the active period of D_{st} and X_l, between their classes and hence a positive flare storm class dependence. The measure representations of D_{st}, a_p, and X_l are multifractal, just as the raw data are. In the selected range of values for K, the multifractal curves do not change noticeably, meaning that the choice of values of K does not affect the results on scaling and class dependence.

[34] **Acknowledgments.** This research was partially supported by the Australian Research Council grant DP0559807, the NSF-CMG grant 0417676, the Natural Science Foundation of China grant 30570426, and the Fok Ying Tung Education Foundation grant 101004. The authors wish to thank the referee for pointing out an important issue on DFA and fractional Brownian motion and other comments and suggestions.

[35] Amitava Bhattacharjee thanks the reviewers for their assistance in evaluating this paper.

References

Anh, V. V., Z. G. Yu, J. A. Wanliss, and S. M. Watson (2005), Prediction of magnetic storm events using the D_{st} index, *Nonlinear Processes Geophys.*, *12*, 799–806.

Anh, V. V., Z. G. Yu, and J. A. Wanliss (2007), Analysis of global geomagnetic variability, *Nonlinear Processes Geophys.*, *14*, 701–708.

Anh, V. V., J. M. Yong, and Z. G. Yu (2008), Stochastic modeling of the auroral electrojet index, *J. Geophys. Res.*, *113*, A10215, doi:10.1029/2007JA012851.

Chen, Z., P. C. Ivanov, K. Hu, and H. E. Stanley (2002), Effect of nonstationarities on detrended fluctuation analysis, *Phys. Rev. E*, *65*, 041107, doi:10.1103/PhysRevE.65.041107.

Chhikara, R. S., and J. L. Folks (1989), *The Inverse Gaussian Distribution*, CRC, Boca Raton, Fla.

Grassberger, P., and I. Procaccia (1983), Characterization of strange attractors, *Phys. Rev. Lett.*, *50*, 346–349.

Halsy, T., M. Jensen, L. Kadanoff, I. Procaccia, and B. Schraiman (1986), Fractal measures and their singularities: The characterization of strange sets, *Phys. Rev. A*, *33*, 1141–1151.

Howard, T. A., and S. J. Tappin (2005), Statistical survey of earthbound interplanetary shocks: Associated coronal mass ejections and their space weather consequence, *Astron. Astrophys.*, *440*, 373–383.

Hu, K., P. C. Ivanov, Z. Chen, P. Carpena, and H. E. Stanley (2001), Effect of trends on detrended fluctuation analysis, *Phys. Rev. E*, *64*, 011114, doi:10.1103/PhysRevE.64.011114.

Jurac, S., and J. D. Richardson (2001), The dependence of plasma and magnetic field correlations in the solar wind on geomagnetic activity, *J. Geophys. Res.*, *106*, 29,195–29,206.

Kantelhardt, J. W., S. A. Zschiegner, E. Koscielny-Bunde, A. Bunde, S. Havlin, and H. E. Stanley (2002), Multifractal detrended fluctuation analysis of nonstationary time series, *Physica A*, *316*, 87–114.

Lui, A. T. Y. (2002), Multiscale phenomena in the near-Earth magnetosphere, *J. Atmos. Sol. Terr. Phys.*, *64*, 125–143.

Liu, H., H. Lühr, S. Watanabe, W. Köhler, and C. Manoj (2007), Contrasting behavior of the thermosphere and ionosphere in response to the 28 October 2003 solar flare, *J. Geophys. Res.*, *112*, A07305, doi:10.1029/2007JA012313.

Mendillo, M., et al. (1974), Behavior of the lonospheric *F* rigion during the great solar flare of August 7, 1972, *J. Geophys. Res.*, *79*, 665–672.

Movahed, M. S., G. R. Jafari, F. Ghasemi, S. Rahvar, and M. R. R. Tabar (2006), Multifractal detrended fluctuation analysis of sunspot time series, *J. Stat. Mech. Theory Exp.*, *2*, 02003.

NiKias, C. L., and M. Shao (1995), *Signal Processing With Alpha-Stable Distributions and Applications*, John Wiley, New York.

Nolan, J. P. (2009), Stable Distributions: Models for Heavy Tailed Data, Birkhauser, Boston, in press.

Park, Y. D., Y.-J. Moon, I. S. Kim, and H. S. Yun (2002), Delay times between geoeffective solar disturbances and geomagnetic indices, *Astrophys. Space Sci.*, *279*, 343–354.

Peng, C. K., S. V. Buldyrev, S. Havlin, M. Simons, H. E. Stanley, and A. L. Goldberger (1994), Mosaic organization of DNA nucleotides, *Phys. Rev. E*, *49*, 1685–1689.

Picoli, S., Jr., R. S. Mendes, L. C. Malacarne, and A. R. R. Papa (2007), Similarities between the dynamics of geomagnetic signal and of heartbeat intervals, *Europhys. Lett.*, *80*, 50006, 1–6.

Schwenn, R., A. Dal Lago, E. Huttunen, and W. D. Gonzalez (2005), The association of coronal mass ejections with their effects near the Earth, *Ann. Geophys.*, *23*, 1033–1059.

Temerin, M., and X. Li (2002), A new model for the prediction of D_{st} on the basis of the solar wind, *J. Geophys. Res.*, *107*(A12), 1472, doi:10.1029/2001JA007532.

Temerin, M., and X. Li (2006), D_{st} model for 1995–2002, *J. Geophys. Res.*, *111*, A04221, doi:10.1029/2005JA011257.

Wanliss, J. A., V. V. Anh, Z. G. Yu, and S. Watson (2005), Multifractal modelling of magnetic storms via symbolic dynamics analysis, *J. Geophys. Res.*, *110*, A08214, doi:10.1029/2004JA010996.

Yermolaev, Y. I., M. Y. Yermolaev, G. N. Zastenker, L. M. Zelenyi, A. A. Petrukovich, and J. A. Sauvaud (2005), Statistical studies of geomagnetic storm dependencies on solar and interplanetary events: A review, *Planet. Space Sci.*, *53*, 189–196.

Yu, Z. G., V. V. Anh, and K. S. Lau (2001a), Measure representation and multifractal analysis of complete genomes, *Phys. Rev. E*, *64*, 031903, doi:10.1103/PhysRevE.64.031903.

Yu, Z. G., V. Anh, and B. Wang (2001b), Correlation property of length sequences based on global structure of complete genome, *Phys. Rev. E*, *63*, 011903, doi:10.1103/PhysRevE.63.011903.

Yu, Z. G., V. V. Anh, K. S. Lau, and L. Q. Zhou (2006), Clustering of protein structures using hydrophobic free energy and solvent accessibility of proteins, *Phys. Rev. E*, *73*, 031920, doi:10.1103/PhysRevE.73.031920.

Yu, Z. G., V. V. Anh, J. A. Wanliss, and S. M. Watson (2007), Chaos game representation of the Dst index and prediction of geomagnetic storm events, *Chaos, Solitons and Fractals*, *31*, 736–746.

Zhang, J., et al. (2007), Solar and interplanetary sources of major geomagnetic storms ($D_{st} \leq -100$ nT) during 1996–2005, *J. Geophys. Res.*, *112*, A10102, doi:10.1029/2007JA012321.

V. Anh and Z.-G. Yu, School of Mathematical Sciences, Queensland University of Technology, GPO Box 2434, Brisbane, Qld 4001, Australia. (v.anh@qut.edu.au; z.yu@qut.edu.au)

R. Eastes, Florida Space Institute, University of Central Florida, Orlando, FL 32816-2370, USA. (reastes@mail.ucf.edu)